



## When probabilistic seismic hazard climbs volcanoes: the Mt Etna case, Italy. Part II: computational implementation and first results

Laura Peruzza<sup>1</sup>, Raffaele Azzaro<sup>2</sup>, Robin Gee<sup>1,5</sup>, Salvatore D'Amico<sup>2</sup>, Horst Langer<sup>2</sup>, Giuseppe Lombardo<sup>3</sup>, Bruno Pace<sup>4</sup>, Marco Pagani<sup>5</sup>, Francesco Panzera<sup>3</sup>, Mario Ordaz<sup>6</sup>, Miguel Leonardo Suarez<sup>6</sup>, Giusy Tusa<sup>2</sup>

<sup>1</sup>Istituto Nazionale di Oceanografia e di Geofisica Sperimentale – OGS, Sgonico (TS), 34010, Italy

<sup>2</sup>Istituto Nazionale di Geofisica e Vulcanologia (INGV), Sezione di Catania – Osservatorio Etno, 95123, Italy

<sup>3</sup>University of Catania, Dep. of Biological, Geological and Environmental Science, Catania, 95129, Italy

<sup>4</sup>DiSPUTer, Università “G. d’Annunzio” Chieti-Pescara, 66013, Chieti, Italy

<sup>5</sup>GEM Foundation, Pavia, 27100, Italy

<sup>6</sup>UNAM, Coyoacan 04510, CDMX, Mexico

Correspondence to: L. Peruzza ([lperuzza@inogs.it](mailto:lperuzza@inogs.it))

**Abstract.** This paper describes the model implementation and presents results of a probabilistic seismic hazard assessment (PSHA) for the Mt Etna volcanic region in Sicily, Italy considering local volcano-tectonic earthquakes. Working in a volcanic region presents new challenges not typically faced in more standard PSHA, which are most broadly due to the nature of the local volcano-tectonic earthquakes, the cone shape of the volcano, and the attenuation properties of seismic waves in the volcanic region. These have been accounted for through the development of a seismic source model that integrates data from different disciplines (historical and instrumental earthquake datasets, tectonic fault data, etc. presented in a companion paper Part I, Azzaro et al., 2017), and by the development and software implementation of original tools for the computation, such as a new ground-motion prediction equation and magnitude-scaling relationship specifically derived for this volcanic area, and the capability to account for the surficial topography in the hazard calculation, which influences source-to-site distances. Hazard calculations have been carried out using two widely used PSHA software packages (CRISIS, Ordaz et al., 2013; the OpenQuake-engine, Pagani et al., 2014). Results are referred to short to mid-term exposure times (10% probability of exceedance in 5 and 30 years, Poisson and time-dependent) and spectral amplitudes of engineering interest. A preliminary exploration of the impact of site-specific response is also presented for the most densely inhabited region, and the variability in expected ground motion is finally commented. These results do not account for the M>6 regional seismogenic sources that dominate the PSHA at long return periods, but present a different viewpoint that we believe is also relevant for retrofitting of the existing buildings, and for driving impending interventions of risk reduction.



## 1 Introduction

It is well known that volcanoes and earthquakes are associated, and some active volcanoes cause damaging earthquakes (e.g. Azzaro, 2004). Since seismic hazard goes with the expected earthquakes, why can't we usually pinpoint volcanoes on a hazard map? The effects of these shallow, volcanic earthquakes can be overshadowed by stronger tectonic earthquakes in the region, particularly when long exposure periods are considered. Furthermore, due to their low magnitudes and the high attenuation typically exhibited in volcanic regions, most ground-motion prediction equations (GMPE) are not applicable for such events. We faced these challenges, among others, in the seismic hazard study of Mt Etna, one of the most active volcanoes in a long-lasting inhabited area in the Mediterranean. In a few kilometers it is possible to walk from the ancient Greek and Roman temples of the coast, to hostile and deserted summit craters 3.3 km above the sea level. While catastrophic earthquakes and tsunamis occur in eastern Sicily on average every 2-3 centuries, building collapse, casualties, and road interruptions due to shallow, light-to-moderate earthquakes (M4-6) happen much more frequently on the flanks of Mt Etna (e.g. D'Amico et al., 2016). These earthquakes are linked to surficial fault sources that breathe with the tectonic stresses and the volcanic dynamics.

In recent years, several analyses have been undertaken to estimate the short to mid-term (5-30 years) capability of local faults on Mt Etna to generate damaging or destructive earthquakes. Two main approaches have been explored. The first is a probabilistic seismic hazard assessment (PSHA) based on macroseismic data, which uses a historical probabilistic approach (the "site-intensity approach", see Azzaro et al., 2008; 2016a) to determine the localities prone to high seismic hazard at the local/regional scale. The second is a seismotectonic approach, where historical inter-event times of fault ruptures are investigated and used to generate an earthquake rupture forecast (Azzaro et al., 2012; 2013). In this approach, poissonian occurrence probabilities of major earthquakes have been determined, as well as time-dependent occurrence probabilities using a renewal processes that takes into account the time elapsed since the last event. Both approaches have found that the local faults significantly contribute to the seismic hazard around Mt Etna with respect to the larger regional events, when short investigation times are considered.

In 2012 a new project started, namely the DPC-INGV V3 Project (Azzaro et al., 2016b), with one of its targets being a new PSHA for the Etna region, due to local volcano-tectonic earthquakes. Working in the Mt Etna region presents new challenges not typically faced in standard PSHA. These are due to i) the nature of the local volcano-tectonic earthquakes, which are low-magnitude (partially out of the applicability range of most GMPEs) and have large ruptures compared to those predicted by commonly used magnitude scaling relationships (MSR), ii) the cone shape of the volcano, where events are located within the volcanic edifice above the sea level, and therefore the topography (elevation) of Mt Etna must be considered, which in turn affects source-to-site distances in the hazard computation, iii) the attenuation properties of seismic waves in the Mt Etna region, where events exhibit rapid attenuation particularly at high frequencies, and finally iv) heterogeneities in rock properties within the volcanic body, and thus proxies simply based on slope or surface geological mapping are not adequate to represent reliable site-specific effects. To address these challenges, we used two PSHA software



packages (CRISIS, Ordaz et al., 2013; the OpenQuake-engine, Pagani et al., 2014) and developed new software functionalities to incorporate the topographic surface into the hazard calculation by modelling sources and sites above the sea level. We also derived new empirical relationships specifically for Mt Etna, such as a MSR (described more in detail in the companion paper, Azzaro et al., 2017, hereinafter referred to as Part I), and a GMPE presented here. In this paper we summarize the source model, discuss the model implementation, new GMPE and software functionalities, and finally present the hazard results. We hope the results of this study may be integrated into a national, more traditional, regulation framework (e.g., Stucchi et al., 2011), for having realistic and useful ground motion prediction maps devoted to urban planners and structural designers.

## 2 Seismic source model: conceptual components

The seismic source modelling at Mt Etna accounts for different levels of increasing complexity, and sources are modelled using distributed seismicity as well as fault sources. For a full description of the individual model components and the process of defining seismic sources, we refer the reader to Part I. The source model accounts for some basic assumptions concerning the engine of earthquake occurrences, which in a volcanic area can be due to the brittle failure of rock, known as volcano-tectonic earthquakes, or the movement of fluids within the volcano, such as volcanic tremor: i) the damaging, shallow focus earthquakes at Mt Etna are volcano-tectonic earthquakes; ii) these earthquakes, which are mainly concentrated on the southeastern flank of Mt Etna, occur with about decennial frequency (see for example, Azzaro et al., 2012; 2013; Sicali et al., 2014) with or without synchronous volcanic activities; iii) the last major events and interseismic periods have been monitored by a dense, high-quality instrumental local network which geometry and characteristics are essentially remained unchanged during the last two decades (Alparone et al., 2015).

In Part I, we describe in detail the different seismic sources defined for representing the shallow volcano-tectonic seismicity at Mt Etna. These sources were defined after checking that a few years of high quality seismic monitoring, during an interseismic interval, can be representative of the long-term seismic rates of volcano-tectonic faults; this simplification is supported by about two centuries of detailed naturalistic observations and chronicles, describing the seismotectonic evidence, and by the deformation rates derived from geodesy. If we accept this working hypothesis, we can parameterize seismic sources by extrapolating decennial datasets. We can also model by means of point sources faults that are still “unknown” as they are not recognised/mapped at the surface, and we may compute earthquake probabilities using any interarrival time/magnitude-frequency distribution (MFD) thus abandoning the requirements of independency and stationarity of events, needed by the traditionally used Poisson process.

The sources at Mt Etna are set up with a great degree of detail and complexity, and take into account the huge amount of available geological, seismological and geodetic data; they derive from historical observations and from the extensive real-time monitoring available for this area.

The three types of seismic sources depicted in Part I are as follows (Figure 1):



- *area seismic sources* (Figure 1a) which are zones of distributed (uniform) seismicity. These encompass the best-known fault systems on the flanks of Mt Etna. They are defined both in CRISIS and the OpenQuake-engine by a horizontal planar surface, modelled as a series of point sources with spatially extended ruptures. This approach is the same used by the actual seismic hazard map of Italian regulation (MPS04, Stucchi et al., 2011), where the whole volcanic body is enveloped in a single polygonal area;
  - *fault sources* (Figure 1b) which model the main tectonic structures. The geometries are based on surface ruptures and other geological and geophysical investigations. Faults are modelled in the OpenQuake-engine by a mesh of points defined by top and bottom (and optionally middle) edges, whose 3D geometry may change in dip and width and extended ruptures float along strike. In CRISIS, faults can be set up by planes of given coordinate vertices;
  - *point sources* (Figure 1c) which are used to represent distributed (gridded, non-uniform) seismicity. The distributed seismicity is defined in a common manner by CRISIS and the OpenQuake-engine, using point sources with spatially extended ruptures and variable properties (e.g. seismicity, depth).
- In the case of Mt Etna, the sources extend above the sea level to model the earthquakes within the volcanic edifice, and also the faults intersect the topographic surface.
- These sources are combined together to form alternative seismic source models. Three source model branching levels are defined, in order of increasing complexity, to represent the epistemic uncertainties (Figure 2):
- *Source Model Level 1* is composed of area sources only. Four zones of uniform seismicity are parameterized by Gutenberg-Richter (GR) MFDs calibrated on the best quality instrumental catalogue (Alparone et al., 2015) during an inter-seismic period that is considered representative of the long-term seismic behavior observed since the XIX century. Seismicity rates are extrapolated until the maximum magnitude observed in the historical period ( $M_{\max}$  5.2), and effective depths are estimated by the analyses of strain release profiles. The values of parameters entered in both the OpenQuake-engine and CRISIS are given in Table 1.
  - *Source Model Level 2* combines major earthquakes ( $M > 4.5$ ) that are assigned to faults only, with background seismicity that is assigned to area sources as in Level 1 (modelled up to  $M_{\max}$  4.5). The MFDs of faults are Gaussian distributions peaked to the characteristic earthquake models; rates are branched, based on the historical observations only, or constrained by geometrical and geological-kinematic considerations on fault size and slip rate (observed and calculated mean recurrence time  $T_{\text{mean}}$  and maximum magnitude  $M_{\max}$  in Table 2; see Pace et al., 2016 for the method; Part I for results obtained at Mt Etna). In Table 2 we summarize the input data and the results in terms of probabilities of occurrence of the characteristic earthquake, following a memory-less process (Poisson), or introducing the time-dependency of the last event of a Brownian Passage Time model, for both the branches, historical and geological-kinematic. Note that the Pernicana Fault is always modelled as GR, not having historical observations supporting the choice of a characteristic earthquake model.
  - *Source Model Level 3* again assigns the major seismicity to faults, as in Level 2, but background seismicity is modelled by distributed seismicity using scattered point sources (in 3D) with spatially variable G-R rates up to  $M_{\max}$  4.5.



**Table 1: parameters of area seismic sources used in the final computations.**

Seismic Zone	Faults	Depth* (upper/lower)	$b$ -value / $\beta$	$a$ -value/ $a_{M_{min}}$	$M_{min}$	$M_{max}$
FF	Fiandaca	-1.0 / 1.0	$0.84 \pm 0.15$ / 1.934	$1.72 / -0.38$	2.5	4.6
STF-SVF	S. Tecla, S. Venerina	-1.0 / 5.0	$1.13 \pm 0.16$ / 2.602	$2.73 / -0.09$	2.5	5.2
MF-SLF	Moscarello, S. Leonardello	-1.0 / 5.0	$0.91 \pm 0.08$ / 2.095	$2.51 / 0.23$	2.5	4.9
PF	Pernicana	-1.0 / 1.0	$0.64 \pm 0.06$ / 1.474	$2.08 / 0.48$	2.5	4.7
Timpe		-1.0 / 5.0	$0.92 \pm 0.06$ / 2.118	$2.90 / 0.60$		

\*negative depth means above the sea level

5 **Table 2: Parameters of fault sources used in the final computations. Historical:  $M_{obs}$ , maximum observed magnitude;  $T_{ela}$ , elapsed time from the last maximum earthquake;  $T_{mean}$ , mean recurrence time of a maximum earthquake;  $\alpha$ , aperiodicity factor; probabilities, probabilities of a maximum magnitude, poisson in 5 years (pois), time-dependent in the next 5 (BPT 5 y) and 30 years (BPT 30 y). Geological-kinematic:  $M_{max}$ , maximum expected magnitude;  $\sigma M_{max}$ , standard deviation of the maximum expected magnitude  $T_{mean}$ , mean recurrence time of maximum earthquake; the other columns as in Historical.**

Fault	Historical							Geological-kinematic						
	$M_{obs}$	$T_{ela}$	$T_{mean}$	$\alpha$	probabilities			$M_{max}$	$\sigma M_{max}$	$T_{mean}$	$\alpha$	probabilities		
					pois	BPT 5 y	BPT 30 y					pois	BPT 5 y	BPT 30 y
Pernicana (PF)	4.7	15	71	0.42	$5.4$ $e-2$	$1.2$ $e-4$	$8.0$ $e-2$	5.0	0.4	28	1.39	$1.2$ $e-1$	$1.7$ $e-1$	$5.9$ $e-1$
Fiandaca (FF)	4.6	123	71	0.42	$5.4$ $e-2$	$1.4$ $e-1$	$6.1$ $e-1$	4.9	0.4	166	1.38	$2.2$ $e-1$	$2.9$ $e-2$	$1.5$ $e-1$
S. Tecla (STF)	5.2	103	71	0.42	$5.4$ $e-2$	$1.3$ $e-1$	$5.9$ $e-1$	5.3	0.4	53	1.41	$6.6$ $e-2$	$5.5$ $e-2$	$2.7$ $e-1$
S. Venerina (SVF)	4.6	15	71	0.42	$5.4$ $e-2$	$7.5$ $e-5$	$6.6$ $e-2$	5.0	0.4	45	1.40	$7.8$ $e-2$	$1.3$ $e-1$	$5.0$ $e-1$
Moscarello (MF)	4.9	106	71	0.42	$5.4$ $e-2$	$1.3$ $e-1$	$5.9$ $e-1$	5.5	0.5	119	1.76	$2.6$ $e-2$	$3.2$ $e-2$	$1.7$ $e-1$

10



### 3 GMPE at Mt Etna

A key component of any seismic hazard assessment is the propagation of seismic energy from the source to the receiver, accounted for in a heuristic way by GMPEs, as the details of seismic wave propagation are usually unknown. Volcanic areas often exhibit peculiar characteristics expressed by high attenuation of seismic energy, especially for shallow earthquakes.

- 5 Concerning the geological conditions, the Mt Etna volcanic edifice overlies a thick sedimentary substratum with strong lateral heterogeneities (see e.g. Branca et al., 2011; De Gori and Chiarabba, 2005). The foci of the shallow events (focal depth less than 5 km) fall into a depth range above mentioned sedimentary substratum; therefore this hypocentral location affects both the seismic scaling laws (relationship of released seismic energy and size of the source) and the wave propagation phenomena (Patanè et al., 1994; Giampiccolo et al., 2007; see Langer et al., 2016 for a more detailed discussion). Strong differences between shallow and deep events (focal depth greater than 5 km) at Mt Etna can be clearly identified just looking at the waveforms. For similar magnitude and distance, the shallow events have more low frequency content than the deeper ones, where conversely the high frequencies prevail (i.e., Tusa and Langer, 2016). The distinctiveness of the shallow events makes the application of common ground-motion prediction equations used for tectonic areas questionable and inappropriate.
- 15 For the purposes of INGV-DPC V3 Project, we derived a local GMPE focusing on the shallow events at Mt Etna and using the high quality data collected by the numerous seismic broadband stations of the Rete Sismica Permanente della Sicilia Orientale (RSPSO) that have been operating in since 2006. We used the same sample of data as Tusa and Langer (2016, hereafter TL16) the original GMPE developed for this project, but this time consider a different distance metric (hypocentral distance instead of epicentral distance as required to incorporate topography into the calculation, see Section 4). The dataset consists of a set of 1200 three-component recordings acquired during 38 events in the magnitude range  $3.0 \leq M_L \leq 4.3$  with hypocentral distances between 0.5 and 100 km. The data were checked visually at all stations to exclude traces with electronic glitches, and with phenomena of amplitude saturation. As a first step in the processing, the digitized velocity time histories of the horizontal components were baseline corrected, removing offset and the linear trend from the data, and instrument corrected obtaining ground velocity in units of m/s. They were then band-pass filtered using corner frequencies of 0.1 and 25 Hz for the high-pass and low-pass filtering, respectively. The weak motion velocity data were differentiated to calculate acceleration time series. The peak amplitude values of the ground acceleration (PGA) were read on the traces resulting from the geometric mean of the horizontal components (Akkar and Bommer 2010; Akkar et al. 2010; Bindi et al. 2011). For an extensive description of statistical characteristics of the data set, for example, in terms of number of data-magnitude, number of data-recording site class, and distance-magnitude distributions, we direct the readers to TL16. In order to compare our data to those recorded in other regions in Italy (in particular the Italian ITA10 equation by Bindi et al., 2011), our empirical GMPE follows the simplified version of the formulation proposed by Boore and Atkinson (2008):

$$\text{Log}(Y) = a + b_1 M + b_2 M^2 + [c_1 + c_2 (M - M_{ref})] \text{Log} \left( \sqrt{R^2 + h^2} / R_{ref} \right) + c_3 \left( \sqrt{R^2 + h^2} - R_{ref} \right) + e_i S_i + \sigma_T \quad (1)$$



where  $M_{ref}$  is a reference magnitude for magnitude dependence of geometric spreading (here fixed to the mode value of the dataset, equal to 3.6),  $R$  is the hypocentral distance in km,  $R_{ref}$  is reference distance at which the near source predictions are pegged, and  $h$  is a pseudo depth. The multiplier of the logarithmic distance term accounts for the magnitude-dependent ground motion decay and controls the saturation of high-frequency ground motions at short distances.  $S_i$  indicates the soil conditions, with  $i$  standing for the soil classes A, B, C, and D defined in the EC8 building code. The  $S_i$  variables of Boolean type are set to unity if the corresponding soil class is met at a site, whereas the  $S_i$  for all other classes is zero. Finally,  $\sigma_T$  represents the total standard deviation, which is the uncertainty in  $\text{Log}(Y)$ . The basic difference with TL16 is the distance metric, measured with respect to the hypocenter instead of the epicenter. This change allows accounting for the elevation of the seismic stations, which may vary in the range of about 2.5 km, a relevant difference, in particular for areas close to the epicenter.

The coefficients of our model were estimated applying the non-linear least-squares Marquardt-Levenberg algorithm as implemented in MATLAB. The coefficients of the model are computed by using an iterative least squares estimation, with specified initial values. In particular, we tested different starting models in order to evaluate their effects on the solution, and at the same time, to select those values towards which the several inversions converged. The equations are derived from the regression analyses for horizontal PGA and 5% damped spectral acceleration (PSA) at several periods from 0.1 to 10 s. The regression coefficients and their 95% confidence intervals for PGAs are reported in Table 3 and for PSAs in the Electronic Supplement. The standard deviation obtained by bootstrap analysis (by resampling our data set 1000 times) is given too. The bootstrap bypasses problems in estimating uncertainties of model parameters obtained in non-linear inversion, which is based on the Jacobian matrix and has the advantage of being applicable without a priori knowledge of the distribution of the underlying parent population. Compared to standard methods, the bootstrap yields a more robust and conservative estimation of parameter uncertainties. The total standard deviation,  $\sigma_T$ , can be split into two terms:

$$\sigma_T = \sqrt{\sigma_{eve}^2 + \sigma_{intraeve}^2} \quad (2)$$

where  $\sigma_{eve}$  and  $\sigma_{intraeve}$  are the inter-event and intra-event error components, respectively representing the error variability for different stations recording the same event, and the error variability for different earthquakes recorded by the same station. Similarly, if the variability among recording sites is taken into account, the total standard deviation of  $\text{Log}(Y)$  in Eq. (1) is given by:

$$\sigma_T = \sqrt{\sigma_{sta}^2 + \sigma_{intraSta}^2} \quad (3)$$

where  $\sigma_{sta}$  and  $\sigma_{intraSta}$  represent the inter-station and intra-station component of the variance. We estimated the inter-group (inter-event and inter-station) and the intra-group (intra-event and intra-station) variance - understood here in terms of mean square errors - for each attenuation model, by applying the “Analysis Of Variance” test. We observe that the horizontal PGA has similar  $\sigma_{eve}$  and  $\sigma_{sta}$  values, whilst the spectral acceleration shows, in general, higher inter-station variability than the inter-event component, suggesting that the local site effects are the main source of ground-motion variability for our data.



In Figure 3 we compare the predictions of horizontal PGA obtained in this study (coefficients reported in Table 1) with those derived by TL16 for shallow seismic activity at Mt Etna, and by Bindi et al. (2011, referred as ITA10) for the whole Italian national territory. Differences between the epicentral (TL16) and hypocentral versions of the GMPE (red and blue curves, respectively) are most evident for source-to-site distances  $< 5$  km, where the hypocentral version of the GMPE predicts higher accelerations. ITA10 (green curves) shows evident differences related to the flat part of the attenuation curves at short distances that goes from 0 to 10 km and more. The extension of this plateau depends critically on the  $h$  parameter, and focal depths in ITA10 are larger than the one selected for Mt Etna, thus leading to a higher  $h$  coefficient. Note that ITA10 is based on 793 records from 99 events and 150 stations, collected on the whole Italian territory; our data set offers at least the same or even a better statistical stability, both from the total number of records (1200) and coverage (records per event, records per station and homogeneity from a seismotectonic point of view). From a practical point of view, the use of ITA10 strongly overestimates the PGA for shallow earthquakes at Mt Etna as it predicts about the same values near the source (distances  $< 2$ -3 km) but much higher values (1-2 order of magnitude) at distances of 5-50 km. A quite different picture is obtained when spectral accelerations are taken into account, for example at  $T > 0.5$  s, where ITA10 shows an underestimation of ground shaking (see Figure 1 in the Electronic Supplementary Material). This is due to the fact the spectra of shallow events at Mt Etna are richer in low frequencies than the earthquakes normally used in GMPE, that are located at depth into the crystalline basement.

**Table 3: Coefficients of Eq. (1) for the prediction of PGAh (gal) for the GMPE in this study. CI95 indicates the confidence intervals at 95% confidence level.  $R^2$  is the determination coefficient.  $\sigma_{eve}$  and  $\sigma_{sta}$  inter-event and inter-station terms of the errors, respectively.  $BS_{mean}$  and  $BS\sigma$  are the mean value and the standard deviation of each coefficient, respectively, estimated by applying the bootstrap technique.**

	<b>a</b>	<b>b<sub>1</sub></b>	<b>b<sub>2</sub></b>	<b>c<sub>1</sub></b>	<b>c<sub>2</sub></b>	<b>h</b>	<b>c<sub>3</sub></b>	<b>e<sub>B</sub></b>	<b>e<sub>D</sub></b>	<b>R<sup>2</sup></b>	<b><math>\sigma_{eve}</math></b>	<b><math>\sigma_{sta}</math></b>	<b><math>\sigma_T</math></b>
	<b>0.329</b>	<b>0.105</b>	<b>0.076</b>	<b>-2.111</b>	<b>0.039</b>	<b>1.553</b>	<b>0.006</b>	<b>0.450</b>	<b>0.457</b>	<b>0.853</b>	<b>0.228</b>	<b>0.222</b>	<b>0.394</b>
<b>CI95</b>	-1.993	-1.136	-0.097	-2.376	-0.125	0.084	0.003	0.337	0.309				
	2.651	1.346	0.248	-1.847	0.204	3.190	0.010	0.562	0.604				
<b>BS<sub>mean</sub></b>	0.381	0.073	0.080	-2.106	0.040	1.174	0.006	0.455	0.463				
<b>BS<sub>σ</sub></b>	1.039	0.554	0.078	0.140	0.078	2.780	0.002	0.076	0.084				

The GMPE equations obtained by this study have been implemented in the software packages used for our analyses, and will be referred to hereinafter as the ETNAhy GMPE model. In CRISIS, the ETNAhy GMPE has been used by means of precompiled attenuation tables: an example for PGA, SA at 0.2, 0.4 and 1.0 s for soil type A is given as a supplementary material. Note that the magnitude range of applicability (stated in this sample table at 2.6-5.3) covers values usually not represented by standard GMPEs. In the OpenQuake-engine, ETNAhy has been added to the extensive library of GMPEs where it is included in the file `tusa_langer_2016.py` ([https://github.com/gem/oq-hazardlib/blob/master/openquake/hazardlib/gsim/tusa\\_langer\\_2016.py](https://github.com/gem/oq-hazardlib/blob/master/openquake/hazardlib/gsim/tusa_langer_2016.py)), which also includes TL16, the version for  $R_{epi}$ .



Verification of the implementation was performed by testing the expected mean and standard deviation output of the GMPE against a table of expected values provided by the authors for different combinations of input variables (e.g. magnitude, distance, and  $V_{s30}$ ).

#### 4 Accounting for topography

5 Another implementation we have done for this study concerns the capability of taking into account the topography (elevation) in PSHA calculation. Typically in PSHA, the sites of the hazard computation are defined in terms of their geographic coordinates on a planar surface representative of the sea level. This implies that the elevations of the sites are assumed to be zero, and the source-to-site distances in the PSHA calculation are computed accordingly. Usually this is an appropriate approximation because the elevations of the sites are small compared to the depths of the sources. However, in  
10 the case of Mt Etna, this approximation cannot be made. Here, the earthquakes are shallow (mostly within the upper 5 km, and some inside the volcanic edifice above the sea level) and the elevation of the volcano increases sharply moving from the coast to the central craters, which are located more than 3 km above sea level. A schematic diagram is shown in Figure 4.

In order to correctly compute the source-to-site distances at Mt Etna, we implemented the possibility to model a 3D topographic surface into both software packages. In CRISIS, this functionality has been added since the release V1.0 of  
15 2015, by means of a specific layer that represents the topography of the study area. A digital elevation model, given in a gridded data file, can be uploaded and the sites elevations are automatically computed on this surface (Figure 5). The capability in the OpenQuake-engine has been available since early 2017 (V2.3.0), and enables the user to specify the sites of the hazard calculation in terms of longitude, latitude, and depth coordinates with respect to the sea level, for example, in the form of a csv file. In both software packages, sources may also be defined above the sea level, using the convention of  
20 negative values for indicating elevations above sea level.

This new functionality can be extended to other regions, although is most appropriate in cases when the inclusion of topography is relevant to hazard (i.e. shallow sources with respect to the topographic elevation, see for example Peruzza et al., 2016), and source locations are well-constrained with respect to the sea level, as is the case at Mt Etna. In theory, site locations may also represent surfaces that are not exposed (e.g. the sea bottom, or bedrock lying below alluvial deposits),  
25 thus opening new potentialities for integrating site-specific response into hazard computation. As incremented capabilities may also introduce new problems for Mt Etna analyses (i.e. how to account correctly for bedrock response, if we are not in free-field conditions), we will accept the simplification that the topographic surface represents reference sites on bedrock.

We performed sensitivity tests at Mt Etna to compare the software performances, and to show the contribution of topography to the hazard. CRISIS and the OpenQuake-engine behave the same in the simplest source formulation, e.g. area and point  
30 sources, and very similarly when complex faults are treated. To demonstrate the influence of topography, we use the same area sources as this hazard assessment but assign all of them the same MFD and a depth of 2.5km, with the seismogenic layer extending from 0 - 5 km (Figure 6). We find that including topography causes an increase in source-to-site distance,



and therefore a decrease in hazard that locally reaches about 50% of the values compared to the model that does not include topography. This effect is most pronounced in the regions of maximum elevation, notably the sources closest to the central craters (i.e. the Pernicana area source).

### 5 Accounting for site-specific response

5 We investigated the site-specific seismic response of the most densely populated area of SE flanks at Mt Etna by adopting the commonly used horizontal to vertical spectral ratio techniques that evaluate the site response properties using both earthquake (HVSr) and ambient noise (HVNR) as input signals. The HVSr were performed selecting 30 local events that occurred in the volcanic area with  $M_L > 2.5$ ; records are extracted from the INGV - Osservatorio Etneo database, while location and magnitude are taken from the INGV - Osservatorio Etneo bulletins. Recorded earthquakes were base-line  
10 corrected, with the purpose of removing spurious offsets, and band-pass filtered in the range 0.08-20 Hz, with a fourth order causal Butterworth filter. The analysis was performed by using 20s time windows, starting from the S-wave onset, including part of the coda and using a 5% cosine-tapered window. Fourier spectra were smoothed using a Konno-Ohmachi filter and the selected time window was compared with the pre-event noise, in order to select good quality data based on the signal/noise ratio. For each recording, only those signals with  $s/n \geq 3$  were considered for analysis. The spectral ratios were  
15 evaluated at each station for the selected events and a geometric mean of all spectral ratios were computed to obtain the mean HVSr curve and the corresponding standard deviation. The resulting experimental HVSr were inverted through ModelHVSr Matlab routines (Herak, 2008) in order to compute theoretical HVSr in homogeneous and isotropic layers. For the 19 considered seismic stations at Mt Etna (stations location in inset map of Figure 7a), the stratigraphic sequence and local velocity model were made by integrating literature information and observations (Azzaro et al., 2010; Branca et al.,  
20 2011; Branca and Ferrara, 2013; Panzera et al., 2011; Panzera et al., 2015; Priolo, 1999). The soil models consist of a number of visco-elastic layers, stacked over a half-space, each of them being defined by the thickness (h), the velocity of the body waves ( $V_p$  and  $V_s$ ), the density ( $\rho$ ), and the Q-factor, which controls the inelastic properties. The incoming waves are assumed to be travelling vertically and assuming that horizontal and vertical motions at the bedrock have no amplification, the HVSr at the surface is then obtained as the ratio between the theoretical transfer functions of S and P waves. The  
25 obtained HVSr output models were then used as input for the amplification function (AF) for 14 seismic stations. Five stations, showing lack of convergence between experimental and theoretical model, were removed. The AFs were computed through frequency-domain calculations, using the program SiteAmp by Boore (2003) that convert a velocity and density model into site amplifications. In particular, the Fortran code calculates the Thomson-Haskell plane SH-wave transfer function for horizontally stratified constant velocity layers at a specific incidence angle within a uniform velocity half-space.  
30 The input parameters are the  $V_s$ , the density ( $\rho$ ), and Q. The half-space is set at the deepest measured layer and the solution is exactly equivalent to the solution computed by the equivalent linear site response program SHAKE for linear modulus



reduction and damping curves (Schnabel et al., 1972). The code computes the amplifications either at specified frequencies or at frequencies corresponding to the “breakpoints” in the velocity model.

The obtained AF were grouped, according to their different “spectral shape” into four classes, by considering the frequency at which the dominant HVSR peak occurs, using the following criteria:

- 5 • ET-1 class: Flat spectral ratios showing amplitude values not exceeding 2 units (including standard deviation);
- ET-2 class: HVSR having fundamental period  $T \leq 0.2$  s with amplitude exceeding 2 units;
- ET-3 class: HVSR with fundamental period  $0.2 < T \leq 1.0$  s with amplitude exceeding 2 units;
- ET-4 class: HVSR showing broadband amplitude exceeding 2 units;

The class’ AF is obtained by averaging the AFs of all the stations included in the class (Figure 7b).

- 10 The good matching obtained by the comparison of experimental HVSRs and HVNRs at the seismic stations located all around the volcano encouraged us to consider the ambient noise signal as a valid seismic input, to be used to define the fundamental frequency of a site. We therefore proceeded to obtain the fundamental period classification in a study area located along the eastern flank of Mt Etna that includes, from North to South, the villages of Piedimonte Etneo, Fiumefreddo di Sicilia, Mascali, Giarre, Riposto, Sant’Alfio, Milo, Zafferana, Santa Venerina, Acireale, Aci Catana, Aci Sant’Antonio,
- 15 Viagrande and Trecastagni (Figure 7a, coloured dots). The fast and inexpensive HVNR technique has been performed by 130 georeferenced noise measurements recorded using a three components velocimeter, on a grid of sites quite homogeneously spaced at about 1x2 km distance. All the HVNRs in the present study were performed using time series of 30 minutes length, with a sampling rate of 128 Hz. Signals were processed by considering time windows of 30 s, selecting the most stationary part, excluding transients associated to very close sources. In this way, the Fourier spectra were
- 20 calculated in the frequency range 0.1-30.0 Hz and smoothed using a proportional 20% triangular window. Following the criteria suggested by the European project Site EffectS assessment using Ambient Excitations (SESAME, 2004), only the spectral ratio peaks having amplitude greater than two units, in the frequency range 0.5-10 Hz, were considered significant. The obtained HVNRs were manually classified and repeatedly checked into the four classes of predominant period previously identified.
- 25 A preliminary predominant-period site classification along the Mt Etna eastern flank is finally attempted, to overcome the one based on average shear wave velocity classification of the upper 30 m ( $V_s30$ ); we mapped in the format required by CRISIS the coefficients to be used in site-specific seismic hazard map, after interpolation of amplification factors at some spectral ordinates done by Nearest Neighbour algorithm (Figure 8). According to Barani and Spallarossa (2016), this soil hazard method can be ascribed to the hybrid probabilistic-deterministic methods, and it may be useful to provide a first
- 30 representation of seismic soil hazard at the large scale.



## 6 Results

In this section, we present the results obtained at Mt Etna, accounting for the branching level of sources (Figure 2), and computational implementations previously described. Seismic hazard maps are referred to rock conditions (Figures 9-11), and exploratory site-specific results are also given (Figure 12).

5 We calculate the hazard for the eastern flanks of Mt Etna for short-to-mid exposure periods (10% exceeding probability in 5 and 30 years), using the ETNAhy GMPE previously described, the MSR derived for Mt Etna, and for a rock condition where  $V_{s30}=800$  m/s (soil type A). The results obtained with the OpenQuake-engine in terms of PGA are shown in Figures 9 and 10. For a 5 year exposure period at 10% exceedance probability (Figure 9), the maximum PGA (73 gal) is seen in Level 2, when using the geological-kinematic approach under the time dependent assumption (Brownian Time Passage model is used, 10 with the conditional probability of occurrence to the time elapsed since the last characteristic event, see Part I and Pace et al., 2016 for details). We see in general that the geological-kinematic approach gives higher results compared to the historical approach. For a 30 year exposure period (Figure 10), the maximum PGA (274 gal) is seen in both the Levels 2 and 3, when using the geological approach under the Poisson assumption. Again, we observe that the geological approach gives higher results compared to the historical approach (in this exposure time, over 2 times higher), and that hazard is also higher when 15 the occurrence rates on the faults have been derived using the Poisson assumption compared to the time-dependent assumption. Within the Timpe Fault System, for both exposure periods, the Fiandaca fault (FF) dominates the hazard for the historical approach, while for the geological approach the Santa Tecla and Venerina Faults (STF, SVF) dominate the hazard. To give context to these values, the current national hazard map (MPS04, see <http://esse1-gis.mi.ingv.it/>), which also considers regional events not modelled in this analysis, shows a PGA around (0.20 - 0.25 g) for the region of Mt Etna, for an 20 exposure period of 50 years. These values fall between the historical and geological approaches of our analysis given an exposure period of 30 years.

It is possible to combine the results of the different branches in a logic tree. The purpose of the logic tree is to consider different modelling possibilities, meanwhile avoiding duplication of similar models. For this reason, we choose to neglect Level 1 and 2 in our weighting, under the assumption that the same information is contained in Level 3, i.e. the 3D gridded 25 seismicity is a more complex representation of the distributed seismicity in Level 1, and the fault sources are modelled in the same way as in Level 2. For the final logic tree, we therefore weigh the four models in Level 3 equally. Combining the models into final hazard maps, we obtain maximum PGA values of 46 and 176 gal, for exposure periods of 5 and 30 years, respectively. For a 5 year exposure period (Figure 9, “L3 Tree” frame), the hazard is highest around the Pernicana Fault source, while for a 30 year exposure period (Figure 10), the hazard is similarly high around the Pernicana Fault source and also around the Santa Tecla and Venerina Faults. 30

In some models, the hazard pattern may appear concentrated around the middle of the fault sources, resembling the pattern of a point source. This is most notable around the Pernicana Fault using the geological approach for an exposure period of 30 years. This pattern can be explained when fault geometry is small compared to rupture extent (ruptures do not float very



much along the fault surface), coupled with using a GMPE derived in terms of a point source distance metric, such as TL16 which uses  $R_{\text{hypo}}$ . In this case, hazard is calculated with respect to the center of the rupture, and this point moves very little as we float the ruptures along the fault surface, which causes the observed pattern.

The simplest model, Level 1, is also computed for some spectral ordinates (Figure 11) in addition to PGA values (reported in Figures 9 and 10). For the spectral ordinates considered, SA(0.2s) gives the highest hazard, with maximum values of 109 gal and 241 gal, for 10% exceedance probability on exposure periods of 5 and 30 years, respectively. For all the exposure periods and spectral ordinates calculated, the hazard of Level 1 is dominated by the Pernicana area source, but note the relative increase of values in the south-easternmost area of the Timpe, as the spectral ordinate shifts toward lower frequencies. The results using CRISIS confirm these values, and will be used for the site-specific test, given below.

10 Lastly, the amplification factors obtained by instrumental measures in the eastern flank of Etna have been used in CRISIS. They give the first seismic hazard site-specific map based on real response data, and clearly illustrate how amplification due to local site conditions can increase the expected ground motion at rock reference sites. Even if these results are preliminary, they can be considered the first example of a new generation of site-specific seismic hazard maps suitable for defining priorities of retrofitting at a local scale. In Figure 12, site-amplified results at two spectral accelerations (0.2 and 1.0s) for a

15 10% probability of exceedance in 5 and 30 years are given. The obtained values show that the site-specific conditions are by far the most important elements in driving the hazard, and the variability in ground motion introduced alters the spatial correlations of nearby localities. Further studies will deepen these analyses, by checking if these results can bridge the gap existing between the probabilistic physically-based models (like the study presented here), and the ones obtained by means of the observed intensities (Azzaro et al., 2008).

## 20 7 Conclusive remarks

This work presents the first seismic hazard maps specific for a volcano, Mt Etna in Sicily, and the implementations introduced *ad hoc* in two PSHA software packages (CRISIS, Ordaz et al., 2013, and OpenQuake-engine, Pagani et al., 2014). Results are given in terms of acceleration (PGA and spectral ordinates at 0.2, 0.4, and 1.0s) for shorter return periods than those normally used in regulation, i.e. for a 10% exceedance probability in 5 and 30 years (corresponding to return

25 periods of 47-284, respectively) as they are intended to be a tool for prioritization of risk mitigation actions.

The main novelties introduced in this study are:

- The derivation and the introduction of a new GMPE into the software, which accounts for the peculiar propagation properties in the volcanic area: it takes into account hypocentral distance ( $R_{\text{hypo}}$ ) and is used jointly with an original magnitude-rupture relationship (see Part I companion paper, Azzaro et al., 2017), derived from the volcanic dataset;
  - The implementation of new computational capabilities in PSHA software by introducing the rough volcano topography, which both software development teams benefitted from. Accounting for more realistic source-to-site distance can impact results up to 50% of the expected values for the shallowest sources in the near field;
- 30



- The conceptual composition of seismic sources, handled in a framework of increasing complexity. Mt Etna sources are depicted through an extensive analysis of geological, historical and instrumental data, described in detail in Part I. A basic observation is that a high-quality instrumental monitoring obtained during a 10 year interseismic period at Mt Etna is representative of the frequency-magnitude distribution derived from a long historical catalogue. This encouraged us to use this non-declustered catalogue for the seismic sources parameterization, potentially opening the usage of generalized, non-Poissonian models for treating the earthquake generation processes in volcanic areas. Further studies are planned to check the applicability of such assumptions in other contexts.
- The seismic sources have been structured in three independent layers, some of them branching to account for different parameterization (e.g. based on historical or geological constraints, to handle the uncertainty of  $M_{\max}$  for a fault source), or different assumptions (e.g. about time-dependency, using Poissonian stationary rates, or probability rates conditioned to the time elapsed since the last major event, based on simplified Brownian Passage Time distributions). We believe in this way the epistemic uncertainties are properly accounted for.

The values obtained have a higher spatial resolution than the national hazard maps, and those referred to rock conditions (where  $V_{s30}=800$  m/s, i.e. soil type A) are significantly higher than the ones used by regulation, even though they only consider surficial volcano-tectonic sources and do not account for the regional sources capable of releasing  $M>6$  earthquakes like the national hazard maps do. A preliminary modelling of site-specific hazard maps is also attempted on the flank of Mt Etna, where extensive field work has been performed for characterizing local amplification factors. They provide a new picture of expected ground motion, about twice the values assigned to reference rock sites, and are strongly spatially uncorrelated. We hope that these analyses will be deepened and broadened by the extensive microzonation investigations carried out in the frame of DPC activities (e.g. [http://www.protezionecivile.gov.it/jcms/it/piano\\_nazionale\\_art\\_11.wp](http://www.protezionecivile.gov.it/jcms/it/piano_nazionale_art_11.wp)), and integrated into the regulation framework, for having realistic and useful ground motion prediction maps devoted to urban planners and structural designers.

Finally, we hope that components of this work can be useful in the seismic hazard assessment of other volcanic regions.

## 25 Acknowledgements

This study has benefited from funding of the Projects V3-2012 and V3-2014, provided by the Italian Presidenza del Consiglio dei Ministri - Dipartimento della Protezione Civile (DPC). This paper does not necessarily represent DPC official opinion and policies.



## References

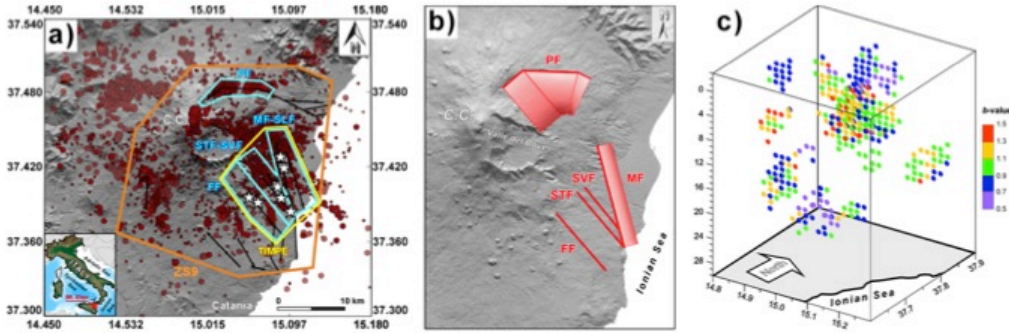
- Akkar S., Bommer J.J.: Empirical equations for the prediction of PGA, PGV and spectral accelerations in Europe, the Mediterranean region and the Middle East. *Seismol Res Lett* 81:195–206, 2010.
- Akkar S., Çağnan Z., Yenier E., Erdoğan Ö., Sandikkaya A., Gülkan P.: The recently compiled Turkish strong motion database: preliminary investigation for seismological parameters. *J Seismol* 14:457–479, 2010.
- Alparone, S., Maiolino V., Mostaccio, A., Scaltrito, A., Ursino, A., Barberi, G., D'Amico, S., Di Grazia, G., Giampiccolo, E., Musumeci, C., Scarfi, L. and Zuccarello, L.: Instrumental seismic catalogue of Mt. Etna earthquakes (Sicily, Italy): ten years (2000-2010) of instrumental recordings, *Annals of Geophysics*, 58, S0435, doi: 10.4401/ag-6591, 2015.
- Azzaro, R.: Seismicity and active tectonics in the Etna region: constraints for a seismotectonic model, In: Mt. Etna: volcano laboratory, A. Bonaccorso, S. Calvari, M. Coltelli, C. Del Negro and S. Falsaperla (eds.), American Geophysical Union, Geophysical monograph, 143, 205-220. 2004.
- Azzaro R, MS Barbano, S D'Amico, T Tuvè, D Albarello, V D'Amico: First studies of probabilistic seismic hazard assessment in the volcanic region of Mt. Etna (southern Italy) by means of macroseismic intensities, *Bollettino di Geofisica Teorica e Applicata* 49 (1), 77-91, 2008.
- 15 Azzaro R., Carocci C.F., Maugeri M., Torrisi A.: Microzonazione sismica del versante orientale dell'Etna studi di primo livello. Ed. Le nove Muse, Catania, pp. 181, 2010.
- Azzaro, R., D'Amico, S., Peruzza, L. and Tuvè, T.: Earthquakes and faults at Mt. Etna (Southern Italy): problems and perspectives for a time-dependent probabilistic seismic hazard assessment in a volcanic region, *Boll. Geofis. Teor. App.*, 53, 75-88, 2012.
- 20 Azzaro, R., D'Amico, S., Peruzza, L. and Tuvè, T.: Probabilistic seismic hazard at Mt. Etna (Italy): the contribution of local fault activity in mid-term assessment, *J. Volcanol. Geoth. Res.*, 251, 158-169, 2013.
- Azzaro R, S D'Amico, T Tuvè: Seismic hazard assessment in the volcanic region of Mt. Etna (Italy): a probabilistic approach based on macroseismic data applied to volcano-tectonic seismicity, *Bulletin of Earthquake Engineering* 14 (7), 1813-1825, 2016a.
- 25 Azzaro, R., and De Rosa, R.: Project V3. Multi-disciplinary analysis of the relationships between tectonic structures and volcanic activity (Etna, Vulcano-Lipari system). Final Report November 1st, 2014 - June 30th, 2015, Agreement INGV-DPC 2012-2021, Volcanological programme 2012-2015: Miscellanea INGV, v. 29, 172 pp., 2016b.
- Azzaro, R., Barberi, G., D'Amico, S., Pace, B., Peruzza, L., and T. Tuvè: When probabilistic seismic hazard climbs volcanoes: the Mt. Etna case, Italy. Part I: model components for sources parametrization. Submitted to NHSS, Special Issue, 2017.
- 30 Barani, S. & Spallarossa D.: Soil amplification in probabilistic ground motion hazard analysis. *Bull Earthquake Eng*, 1-21, doi:10.1007/s10518-016-9971-y, 2016.



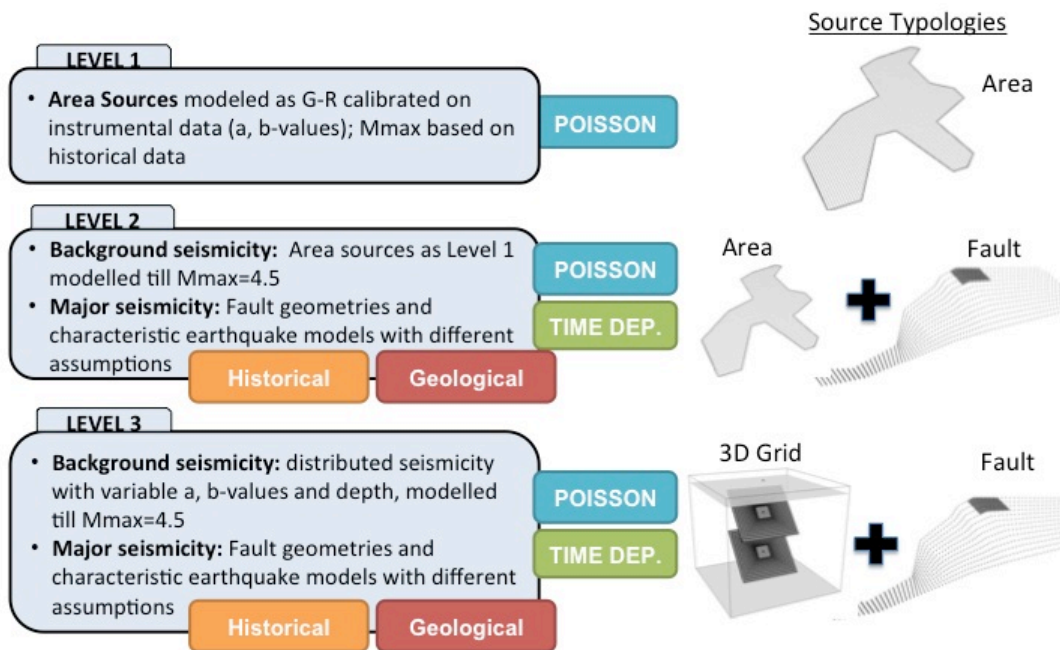
- Bindi D., Pacor F., Luzi L., Puglia R., Massa M., Ameri G., Paolucci R.: Ground motion prediction equations derived from the Italian strong motion database. *Bull Earthq Eng* 9:1899–1920. doi:10.1007/s10518-011-9313-z, 2011.
- Boore D.M.: Prediction of ground motion using the stochastic method. *Pure Appl. Geophys.* 160, 635–676, 2003.
- Boore, D.M., Atkinson, G.M.: Ground-motion prediction equations for the average horizontal component of PGA, PGV, and 5 5 %-damped PSA at spectral periods between 0.01 s and 100 s. *Earthquake Spectra* 24:99–13, 2008.
- Branca S., Coltelli M., Groppelli G.: Geological evolution of a complex basaltic stratovolcano: Mount Etna, Italy. *Ital. J. Geosci.*, 130 (3), 306-317, DOI: 10.3301/IJG.2011.13, 2011.
- Branca S., Ferrara V.: The morphostructural setting of Mount Etna sedimentary basement (Italy): implications for the geometry and volume of the volcano edifice and its flank instability. *Tectonophysics*, doi: 10.1016/j.tecto.2012.11.011, 10 2013.
- D’Amico S, F Meroni, ML Sousa, G Zonno: Building vulnerability and seismic risk analysis in the urban area of Mt. Etna volcano (Italy) *Bulletin of Earthquake Engineering* 14 (7), 2031-2045, 2016.
- De Gori P. Chiarabba C.: Qp structure of Mount Etna: Constraints for the physics of the plumbing system. *J. geophys. Res.*, 110, B05303, doi:10.1029/2003JB002875, 2005.
- 15 Giampiccolo E., D’Amico S., Patanè D., Stefano Gresta: Attenuation and Source Parameters of Shallow Microearthquakes at Mt Etna Volcano, Italy. *Bull. Seism. Soc. Am.*, 184–197, doi: 10.1785/0120050252, 2007.
- Herak M.: ModelHVSR-A Matlab® tool to model horizontal-to-vertical spectral ratio of ambient noise, *Computers Geosciences*, 34, 1514-1526, 2008.
- Langer H., G. Tusa, L. Scarfi, R. Azzaro: Ground-motion scenarios on Mt. Etna inferred from empirical relations and 20 synthetic simulations *Bulletin of Earthquake Engineering*, July 2016, Volume 14, Issue 7, pp 1917–1943, 2016.
- Ordaz M., Martinelli F., D’Amico V. and Meletti C.: CRISIS2008: A flexible tool to perform probabilistic seismic hazard assessment. *Seismological Research Letters* 84, 495-504, 2013.
- Pace, B., Visini, F. and Peruzza, L.: FiSH: MATLAB tools to turn fault data into seismic hazard models, *Seism. Res. Lett.*, 87, 2a, doi: 10.1785/0220150189, 2016.
- 25 Panzera F., Lombardo G., Monaco C., Di Stefano A.: Seismic site effects observed on sediments and basaltic lavas outcropping in a test site of Catania, Italy. *Natural Hazards*, doi: 10.1007/s11069-015-1822-7, 2015.
- Panzera F., Rigano R., Lombardo G., Cara F., Di Giulio G., Rovelli A.: The role of alternating outcrops of sediments and basaltic lavas on seismic urban scenario: the study case of Catania, Italy. *Bulletin of Earthquake Engineering* 9 (2), 411-439, 2011.
- 30 Pagani, M., Monelli, D., Weatherill, G., Danciu, L., Crowley, H., Silva, V., Henshaw, P., Butler, L., Nastasi, M., Panzeri, L., Simionato, M. and Viganò, D.: OpenQuake-engine: An open hazard (and risk) software for the Global Earthquake Model, *Seismol. Res. Lett.*, 85, 692-702; doi:10.1785/0220130087, 2014.
- Patanè, D., F. Ferrucci, S. Gresta: Spectral features of microearthquakes in volcanic areas: attenuation in the crust and amplitude response of the site at Mt Etna, Italy, *Bull. Seism. Soc. Am.* 84, 1842–1860, 1994.



- Peruzza L, R Gee, B Pace, G Roberts, O Scotti, F Visini, L Benedetti, M Pagani: PSHA after a strong earthquake: hints for the recovery, *Annals of Geophysics* 59, 2016
- Priolo E.: 2-D spectral element simulation of destructive ground shaking in Catania (Italy). *J. Seismol.*, 3, 289–309, 1999.
- SESAME: Guidelines for the implementation of the H/V spectral ratio technique on ambient vibrations: Measurements, processing and interpretation. SESAME European Research Project WP12, deliverable D23.12, at <http://sesame-fp5.obs.ujfgrenoble.fr/Deliverables>, 2004.
- 5 Tusa G., Langer H.: Prediction of ground-motion parameters for the volcanic area of Mount Etna. *J Seismol.* doi:10.1007/s10950-015-9508-x, 2016.
- Schnabel, P. B., Lysmer, J. and Seed, H. B.: Shake a computer program for earthquake response analysis of horizontally layered sites. Report No. EERC 72 - 12, Earthquake Engineering Research Center, University of California, Berkeley, California, 1972.
- 10 Sicali, S., Barbano, M.S., D'Amico, S. and Azzaro R.: Characterization of seismicity at Mt. Etna volcano (Italy) by inter-event time distribution, *J. Volcanol. Geotherm. Res.*, 270, 1-9, 2014.
- Stucchi, M., C. Meletti, V. Montaldo, H. Crowley, G.M. Calvi and E. Boschi: Seismic Hazard Assessment (2003- 2009) for the Italian Building Code, *B. Seismol. Soc. Am.*, 101, 1885-1911; doi:10.1785/0120100130, 2011.
- 15



5 Figure 1: source typologies at Mt Etna. a) polygonal area sources representing uniform seismicity: the ones defined in this study (in pale blue and yellow) follow the non-creeping sections of the best-known fault systems; in orange the single area source used in the maps of Italian regulation (ZS9, Stucchi et al., 2011); b) fault sources modelling the main volcano-tectonic structures detected on Etna's flanks (see Table 1 for the nomenclature); the red boxes and lines represent the projection at the surface of the fault planes; c) 3D mesh of point sources, used to model the scattered background seismicity, b-values represented by colors. Details are given in the companion Part I paper (Azzaro et al., 2017).



10 Figure 2: Schematic chart describing the three branching levels of the source model, and depiction of the different source typologies used for modelling. The major seismicity of Level 2 and 3 is modelled using fault sources, where seismicity rates are derived using historical and geological approaches, and both approaches consider both time independence and time dependence.

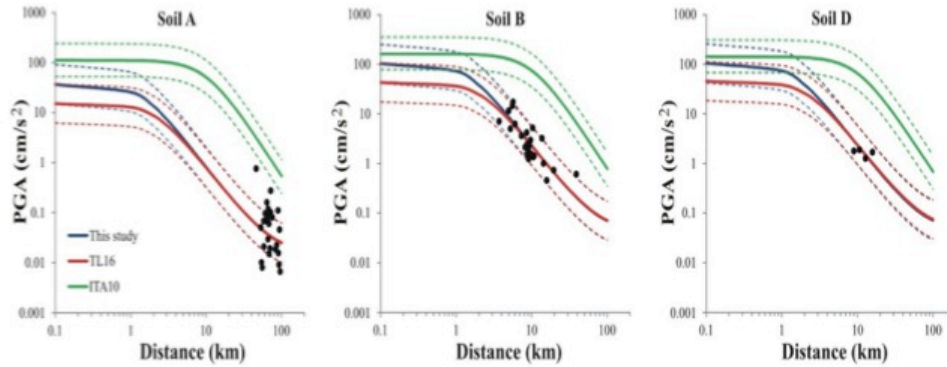


Figure 3: Predicted mean attenuation-curves for a  $M_L=4$  earthquake by the empirical law estimated in this study: ETNAhy, (continuous blue lines), TL16 (continuous red lines), and ITA10 (continuous green line). The dashed lines represent the standard deviation of the mean. The black circles refer to the observations of our dataset with  $3.9 \leq M_L \leq 4.1$ ; the three frames represent the different soil type according to the EC8 Building code.

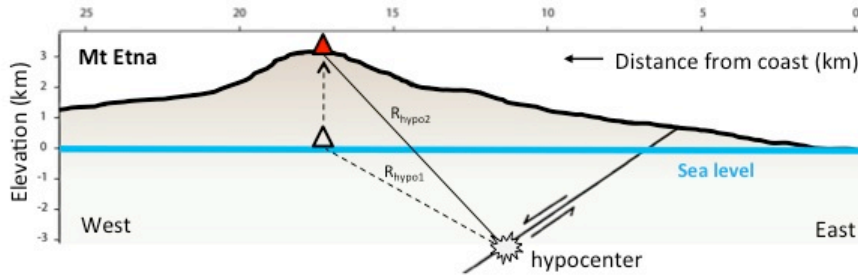
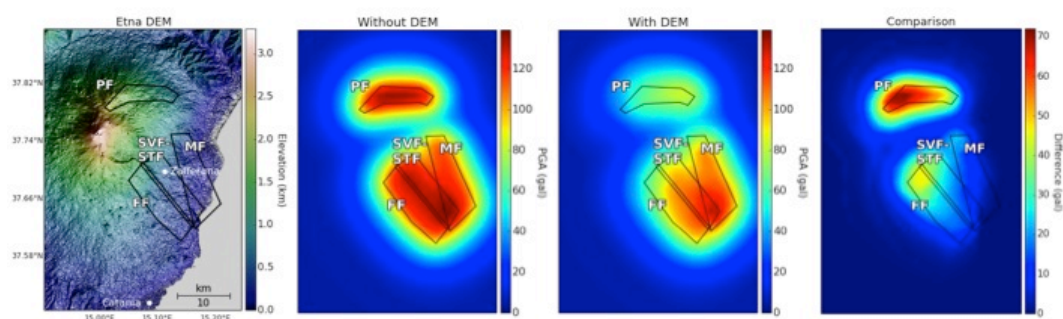


Figure 4: A topographic profile of Mt Etna shown to scale, extending from the western side of the volcano to the eastern coast (Ionian Sea). Using a hypothetical fault, it can be demonstrated how the source-to-site distance increases ( $R_{\text{hypo2}} > R_{\text{hypo1}}$ ) if the site is defined on the topographic surface (red triangle) compared to the sea level (clear triangle).



Figure 5: snapshots of topography and sources in CRISIS: a) DEM at Mt Etna; b) preliminary fault sources in 3d (note the vertices above the sea level, marked by black dotted line in the cross sections).



5 Figure 6: hypothetical example showing the sensitivity of the hazard results to topography using the OpenQuake-engine. The same area sources are used as in this study, except here they are all assigned the same MFD and a depth of 2.5 km. When the sites are defined on a realistic topographic surface, the hazard decreases due to an increase in source-to-site distance.

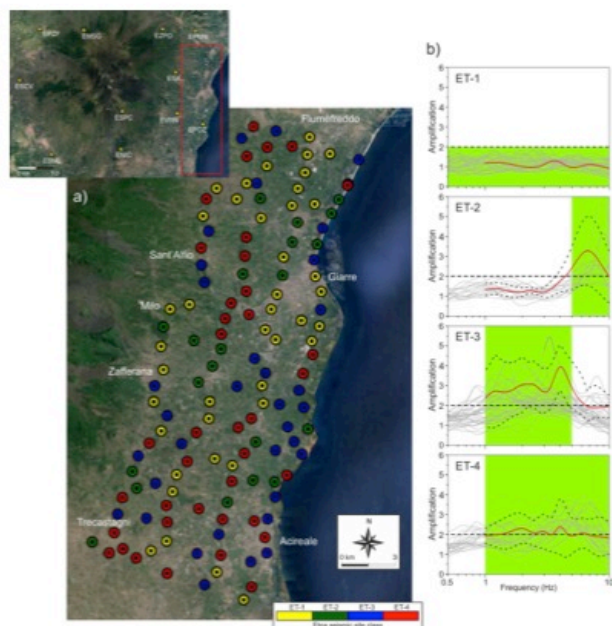
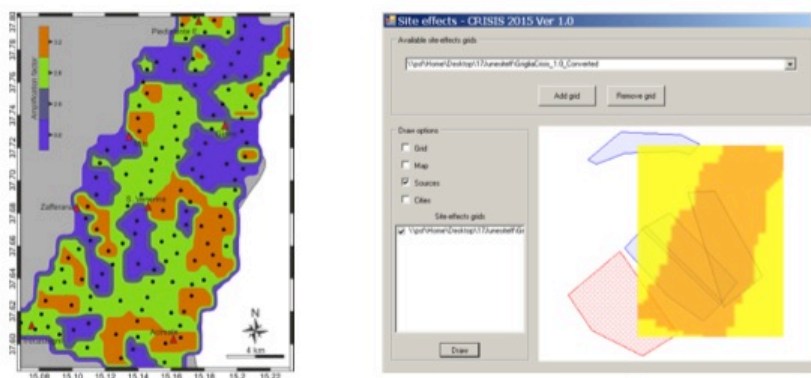


Figure 7: site response along Mt Etna South-eastern flank (in the inset map): a) sites investigated by HVSR/HVNR measurements and simplified spectral classes; b) spectral classes defined by grouping the HVNR curves into four classes based on the frequency of the dominant peak: mean site amplification function by red curve, standard deviation by dashed black curves.



5

Figure 8: simplified site-specific response along Mt Etna South-eastern flank: a) amplification factors at SA(0.2)s, obtained by interpolating the measured sites using the Nearest Neighbour algorithm; b) amplification factors as implemented in CRISIS; orange stripe represents the area where amplification factors will be entered in hazard computations.

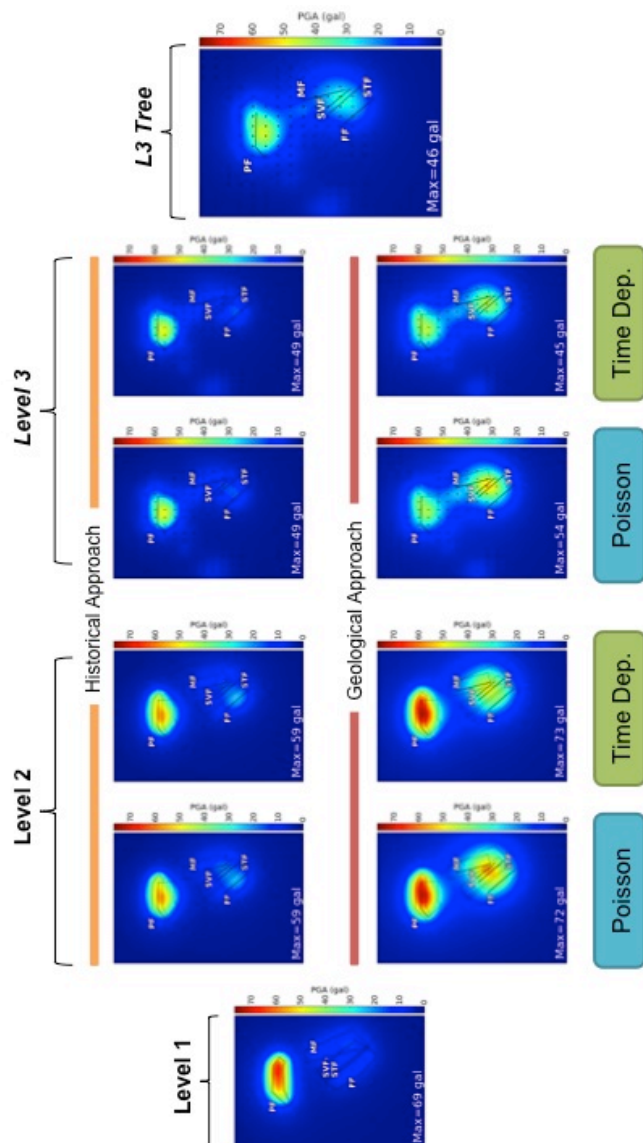


Figure 9: Hazard results for a 10% exceedance probability in 5 years in terms of PGA, when  $V_{s30} = 800$  m/s. Thickest lines indicate fault traces.

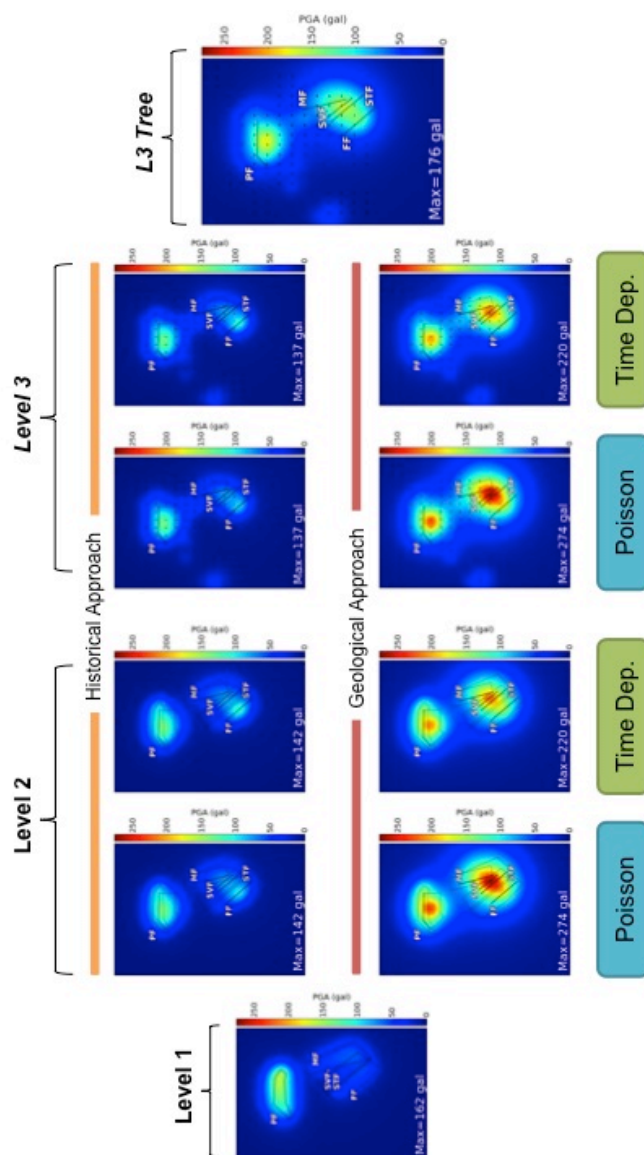


Figure 10: Hazard results for a 10% exceedance probability in 30 years in terms of PGA, when  $V_{30} = 800$  m/s. Thickest lines indicate fault traces.

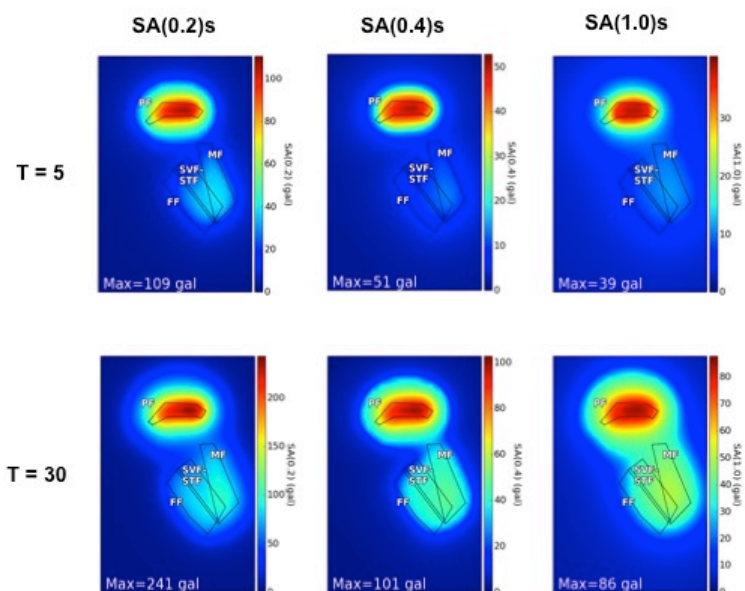
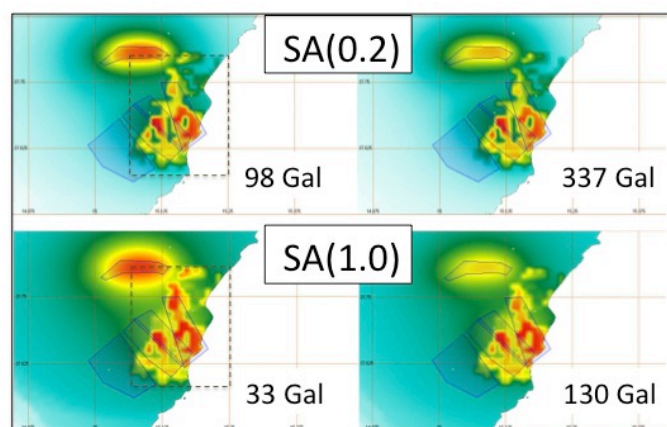


Figure 11: Hazard results of Level 1 at different spectral ordinates for a 10% exceedance probability in 5 and 30 years, and  $V_{30} = 800$  m/s.



5 Figure 12: Site-specific hazard results of Level 1 (CRISIS): in the upper frames, the maps of SA(0.2s) at 10% exceedance probability in 5 (left) and 30 years (right) are obtained for  $V_{30} = 800$  m/s for the whole area; the amplification factors are applied on a stripe on Mt Etna South-eastern flank (dashed black rectangle, see details in Figures 7, 8); the lower frames refer to SA(1.0s).